International Journal of Environmental, Social and Economic Sustainability
www.ijeses.org

D. Dauda et al., Vol. 1, No. 1, March, 2026 | Research Article

Rotor Angle Stability Analysis of Hybrid Wind Energy Source Integrated with Conventional Grid

Dahiru Dauda*‡, Aliyu Sabo**, Abdulmalik Ibrahim Dabo ***, Kenneth Okedu ****, Noor Izzri Abdulwahab*****

*,**,***Department of Electrical and Electronics Engineering, Faculty of Engineering and Engineering Technology, Nigerian Defense Academy, Kaduna, Nigeria

****School of Information Technology and Engineering, Melbourne Institute of Technology, 3000, Victoria, Australia

***** Department of Electrical/Electronic Engineering, Faculty of Engineering, University Putra Malaysia (UPM), UPM Serdang 43400, Selangor, Malaysia

(dauda.dahiru2022@edu.nda.ng, saboaliyu98@gmail.com, abdulmalikdaboi@gmail.com, kokedu@academic.mit.edu.au, izzri@upm.edu.my)

‡Corresponding Author: Dahiru Dauda, Nigerian Defense Academy, dauda.dahiru2022@edu.nda.ng,

Received: 01.02.2026 Accepted: 24.03.2026

Abstract- This paper investigates the design and optimization of a Power System Stabilizer (PSS) to enhance rotor angle stability in a hybrid wind energy system integrated with a conventional grid (single machine infinite bus) under a 50% step disturbance in mechanical torque (Tm). Low damping torque, extended electromechanical oscillations, and rotor instability were the outcomes of the disturbance's torque mismatch between the mechanical input and electrical output. In order to optimize damping performance, the PSS parameters were ideally tuned using the Artificial Ecosystem Based Optimization (AEO) and Secretary Bird Optimization (SBO) algorithms. MATLAB/Simulink 2023a was used to model and simulate the hybrid system, which consists of SMIB, Doubly-Fed Induction Generator (DFIG), and Permanent Magnet Synchronous Generator (PMSG) wind farms. Without a PSS, the system exhibited poor damping with rotor speed deviation and actual rotor speed and system rotor angle settling times of 9.98 s, 8.61 s, and 9.41 s, respectively. The AEO-PSS reduced these to 3.49 s, 2.98 s, and 3.59 s, while the SBO-PSS achieved superior responses of 1.99 s, 2.20 s, and 2.21 s. In the hybrid wind-integrated configuration, the SBO-PSS achieved a rotor speed deviation settling time of 2.20 s, outperforming AEO-PSS at 2.51 s. Eigenvalue analysis confirmed enhanced damping ratio. The optimized SBO-PSS effectively mitigated these effects, improving synchronizing torque and shifting system poles deeper into the left half-plane to ensure stable and robust operation. The 50% Tm torque disturbance, low excitation damping torque, and inertia from wind integration were the main causes of the instability; however, the optimized controller successfully reduced these effects by enhancing synchronizing torque and moving system poles deeper into the left half-plane to guarantee stable and reliable operation.

Keywords: wind energy conversion system, single machine infinite bus system, rotor angle stability, power system stabilizer, secretary bird optimization algorithm

1. Introduction

The availability and technology of wind energy are increasing every day. Because wind energy has significant benefits over fossil fuels, it is becoming one of the main sources of electricity for both household and industrial usage [1]. Modern power system Grids are heavily networked using modern technologies, and control devices are also included in the system to increase economic advantages and efficiency [2]. Concludes that the earth's largest artificial living network is the grid of the electricity system. Due to the rising need for electric energy supply during the past 10 years, integration of

Cite this article as: D. Dauda, A. Sabo, A. I. Dabo, K. Okedu, and N. I. Abdulwahab, "Rotor Angle Stability Analysis of Hybrid Wind Energy Source Integrated with Conventional Grid", International Journal of Environmental, Social and Economic Sustainability, (IJESES), Vol.1, No. 1, pp. 19-35, March, 2026.

major intermittent renewable energy resources, such as wind energy, into the current power system grid has expanded dramatically. Thus, increasing the availability of electric energy and lowering greenhouse gas emissions [3]. The largest wind farm in the world, located in China at Gansu, has a planned capacity of 20 GW. The farm combined permanent magnet synchronous generator turbines with a double-fed induction generator [4]. These two wind turbine technologies, double-fed induction and permanent magnet synchronous generator, are connected by power converters. When power converters are operating at maximum capacity, the PMSG initially costs more than the DFIG, which has a gearbox mechanism and a 20–30% power converter rating [5]. There are obstacles to wind energy's grid integration due to several issues, such as unstable generation, issues with active and reactive power quality, and stability of the electrical system [5]. Since the 1920s, power system stability has been acknowledged as a significant issue for the safe running of systems [6]. Power system stability refers to an electric power system's capacity to regain operational equilibrium following a physical disturbance [7]. Several large blackouts caused by the electrical system's instability have shown the relevance of this problem [8]. Power system stability is the most important component in attaining dependable and safe operation. Due to technological advancements and complexity, there is a significant increase in the need for electricity [9]. Transmission lines are the means by which this ongoing demand is incorporated into electricity networks. To accommodate the growing demand, many power systems are running close to capacity. Power system oscillations can result from any disruption or breakdown on the grid [6]. There might be major risks to the stability of the power system if these oscillations are not entirely dampened [10]. Thus, resolving the oscillation issue in the electricity supply is an international concern. Fast-acting, high-gain automated voltage regulators were first used in the generator excitation system in the early 1960s. By decreasing the damping torque, this further increased the issue of low-frequency electromechanical oscillations, or power system oscillations, in the power system [11]. Low-frequency oscillations are decreased and power system stability is improved by establishing coordination between a power system stabilizer and the excitation control system's automatic voltage regulator [12]. To boost the machine damping torque, PSS adds a signal to the excitation [7]. This process dampens the low-frequency oscillations in the system. PSS raises the angle level [13]. The rotor's power, frequency, or speed are the PSS's inputs. The selection and proper tuning of the PSS and AVR controller parameter values determine the power system's degree of oscillation damping. FOPID (fractional-order PID) controllers, PI controllers, lead-lag controllers, and PID controllers are some of the different types of PSS units. Due to its simplicity and ease of installation, the lead-lag PSS is one of the more traditional and often used PSS [14]. Because the power system is non-linear, a PSS controller with fixed parameters cannot adequately reduce oscillations in the power system [15], [16].

In this study, the design challenge of the suggested PSS is transformed into an optimization problem by using a non-time domain-based objective function for efficient damping operation. To reduce power system oscillations that result from integrating a wind farm of DFIG and PMSG wind turbine generators into the power system grid. The anticipated outcome of this study is a reduction in the power system oscillation inside an integrated power grid system.

1.1. Problem Statement

System stability is threatened by the growing integration of renewable energy sources, like wind, into traditional power systems. Due to the inherent intermittent and unpredictable nature of wind energy generation, variations in mechanical input torque and electrical output power can result in rotor angle instability and electromechanical oscillations. When a 50% step disturbance is introduced to the mechanical torque, the generator experiences prolonged oscillations, reduced damping torque, and a delayed return of synchronism. Power System Stabilizers (PSS) with fixed parameters cannot handle these nonlinear and time-varying dynamics, especially in hybrid configurations involving Doubly-Fed Induction Generator (DFIG) and Permanent Magnet Synchronous Generator (PMSG) systems integrated with a Single Machine Infinite Bus (SMIB) (conventional grid). An adaptive and optimized damping controller is therefore required in order to successfully suppress oscillations and dynamically react to operating conditions. In order to improve damping performance, speed up transient recovery, and improve rotor angle stability in a hybrid renewable integrated power system, this study uses two metaheuristic optimization algorithms: Artificial Ecosystem Optimization (AEO) and Secretary Bird Optimization (SBO).

1.2. Objectives

- To model and simulate a conventional grid system in the MATLAB/Simulink environment.
- To design and optimize a Power System Stabilizer (PSS) using the Secretary Bird Optimization (SBO) algorithm and validate its performance using the Artificial Ecosystem-Based Optimization (AEO) algorithm.
- To create and incorporate a hybrid Wind Energy Conversion technology (WECS) that combines the SMIB technology with models of Permanent Magnet Synchronous Generator (PMSG) and Doubly Fed Induction Generator (DFIG).
- To evaluate system performance through time-domain and eigenvalue analyses under No-PSS, AEO-PSS, and SBO-PSS conditions, focusing on damping improvement, settling time reduction, and stability enhancement.

2. Stability in Power System

Power systems need stability because it guarantees the grid's dependability and security [17]. According to the definition of power system stability, it is the system's capacity to recover from a physical disturbance and reach a state of operational equilibrium with most of its variables limited to ensure the system's overall integrity at a given starting

operating condition. A steady power supply is the most crucial component for attaining safe and dependable operation. Power system oscillation can pose a major danger to an integrated power system's stability. Modern integrated power systems' ability to operate securely is greatly impacted by the efficacy of oscillation damping [18]. The increasing renewable energy penetration, like wind, poses various difficulties that force considerable adjustments in the current power system and threaten the power system stability [19][20].

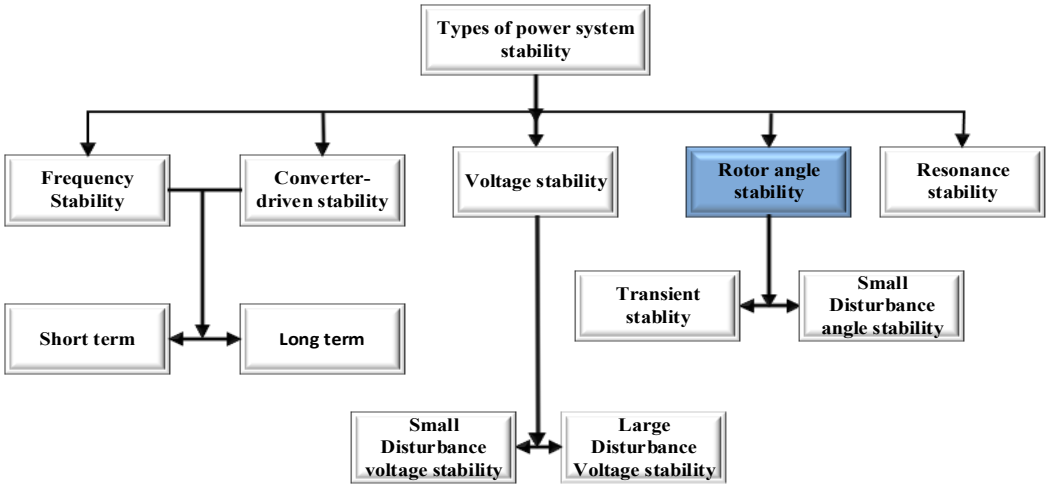

Fig. 1. Types of power system stability.

.

An intrinsic feature of synchronous generators is oscillations in the power system, which cause variations in output power while the rotors spin at synchronous speed. Oscillations in the power system are a fundamental characteristic of an integrated power grid system and are primarily caused by the non-linear nature of synchronous generators. Oscillations in the power network system, which happen as a sequence of connected incidents within a synchronous generator, can be caused by any incident or disturbance in the power system. Under typical operating circumstances, the physical and electromagnetic torque ratio keeps the synchronous generator's rotor speed at synchronism. The rotor's speed changes, either increasing or decreasing from its synchronous speed [11], [21]. Classification is therefore essential to provide a more comprehensive practical analysis and a better solution to power system stability problems. Power system oscillations and the related rotor angle stability problems are the primary focus of this investigation [22].

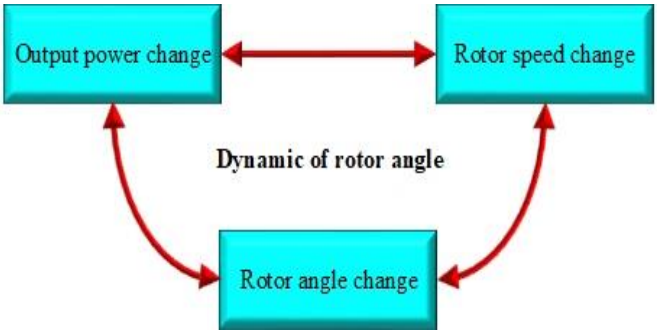

Fig. 2. Dynamic of rotor angle stability.

3. Power Test System

Among these is Kundum, an IEEE power-test system benchmark. Additionally, the SMIB system, which has a single generator and two buses, was converted to a thirteen (13) bus network by integrating WECS at bus 13. Fig. 3 displays a single-line diagram of the updated power-test system.

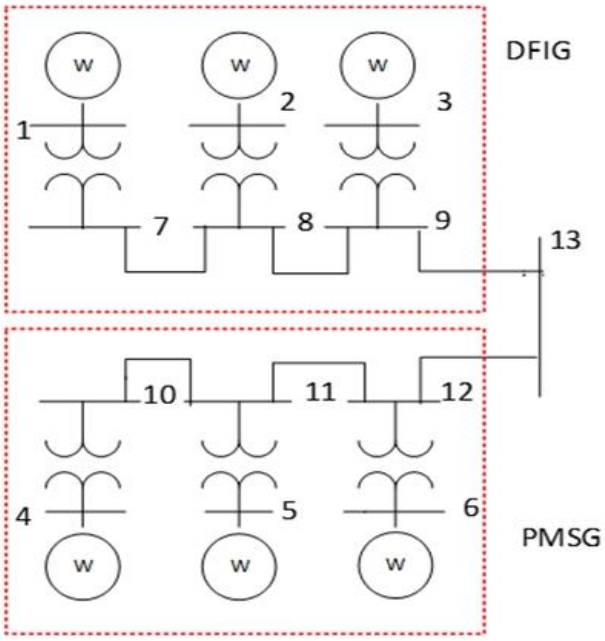

Fig. 3. The Kunju Power test system with WECS.

An infinite bus, which is a bus with a fixed voltage and frequency that is fixed in both magnitude and angle, is referred to as a single machine connected to an infinite bus system. This one machine coupled to an infinite bus is an example of a strong grid connection, meaning that power is added at the connection point to the infinite bus without significantly altering the system's frequency and voltage. A single machine, also known as a synchronous machine, is made up of a fixed component called the stator, which has armature windings, and a spinning component called the rotor, which can be a cylindrical rotor or a salient pole and has field windings [23]. In addition to the d-axis and q-axis symmetry, which IEEE chose for simple analysis and representation of the three-phase balanced voltage generated in the synchronous machine, there is a tiny air gap between these 27 pieces [24],[23]. Time-varying fluxes between the rotor and the stator armature circuits cause inductances (self and mutual) to be induced as the rotating component, the rotor, rotates in relation to the stator circuits. These time-varying inductances make synchronous machine analysis and modeling more difficult, but d-axis and q-axis symmetry dq transformations make the model simpler [7]. The SMIB generator power system is shown in Fig. 4.

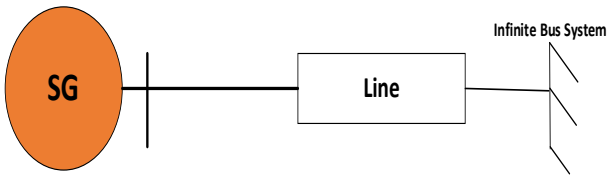

Fig. 4. Single generator.

The techniques applied, as well as the mathematical expressions for the entire system. Existing research served as the basis for the power system mathematic equations representing the systems under study [7], [24].

Excitation System:

The excitation system aids in controlling the power source bus voltage by modifying the generator's field voltage.

$$\frac{dE_{fd}}{dt} = \frac{1}{T_a}(K_a V_{ref} - K_a E_t - E_{fd}) \quad (1)$$

The single-mass system's governing equations are found in eqn. 2 depicts the shift in generator rotor angle brought on by a discrepancy between the network's synchronous speed and the rotor's angular speed. Additionally, the electrical output generates equation 3, which is required to explain the change in the rotor angular speed caused by an imbalance of torques in the mechanical system eqn. 5.

$$\frac{d\delta}{dt} = \omega_b(\omega_r - \omega_s) \quad (2)$$

$$\frac{d\omega_r}{dt} = \frac{1}{2H}\left(T_m - T_e - D(\omega_r - \omega_s)\right) \quad (3)$$

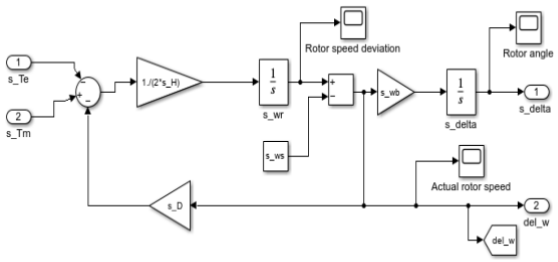

Fig. 5. Simulink representation of torque angle loop.

For a synchronous machine, the rotor speed is normally close to the synchronous speed (ω_s). The system frequency is 60 Hz.

$$\omega_s = 2\pi f = 377 \text{ rad/sec}$$

Rotor speed $\omega(t)$(actual rotor speed) = synchronous speed (ω_s) plus deviation. $\omega(t) = \omega_s + \Delta\omega(t)$

Rotor speed deviation $\Delta\omega(t)$ is the signal that measures how far the rotor is from synchronous speed: $\Delta\omega(t) = \omega(t) - \omega_s$

Synchronous generators employ governor control mechanisms to maintain system frequency under variations in generation–load balance by modifying the mechanical input torque

$$\frac{dT_m}{dt} = \frac{1}{T_g}\left(T_{m2} - T_m - \frac{\omega_r - \omega_s}{R_{gov}}\right) \quad (4)$$

Where E_t represents the magnitude of the generator voltage, E_{fd} is the voltage in the field winding, K_a represents the static excitation gain, V_{ref} is the reference voltage, T_a is the static excitation time constant, δ represents the rotor angle of the generator, ω_s is the generator's synchronous speed, ω_r is the generator rotor angle, ω_b is the base speed value, H is the inertia, T_e and T_m are the electrical and mechanical torques, respectively, D is the self-damping, T_g is the time constant of the governor, R_{gov} is the governor droop, and T_{m2} is the generation load reference.

Synchronous machine:

The electrical side of the generator and the machine equations are separated into electrical torque Te/Pe eqn. (5), the stator current components in eqns. 6 and 7 for the q and d axis damper coil flux linkage caused by transient EMF in the field in eqn. 8, and eqn. 9 for the axis damper coil flux linkage. The axis damper coil flux connection is caused by the sub-transient EMF in eqn. 10. Eqn. 11 represents the d-axis and q-axis flux connection caused by the sub-transient EMF in the field in the q-axis. The DQ conversion gives the rotation terms

for the phasors; here the angle (δ) is transformed *into* $e^{-j\delta}$ *and* $e^{+j\delta}$ equations 12 and 13.

$$T_e = \frac{x''_d - x_{ls}}{x'_d - x_{ls}} E'_q I_q + \frac{x'_d - x''_d}{x'_d - x_{ls}} \psi_{1d} I_q + \frac{x''_q - x_{ls}}{x'_q - x_{ls}} E'_d I_d - \frac{x'_q - x''_q}{x'_q - x_{ls}} \psi_{2q} I_d + (x''_q - x''_d) I_d I_q \quad (5)$$

$$I_q = \frac{R_s}{R_s^2 + x''^2_d} \left(E'_q \frac{x''_d - x_{ls}}{x'_d - x_{ls}} + \psi_{1d} \frac{x'_d - x''_d}{x'_d - x_{ls}} - V_q \right) + \frac{x''_d}{R_s^2 + x''^2_d} \left(E'_d \frac{x''_q - x_{ls}}{x'_q - x_{ls}} - \psi_{2q} \frac{x'_q - x''_q}{x'_q - x_{ls}} - V_d \right) \quad (6)$$

$$I_d = \frac{R_s}{R_s^2 + x''^2_d} \left(E'_d \frac{x''_q - x_{ls}}{x'_q - x_{ls}} - \psi_{2q} \frac{x'_q - x''_q}{x'_q - x_{ls}} - V_d \right) - \frac{x''_d}{R_s^2 + x''^2_d} \left(E'_q \frac{x''_d - x_{ls}}{x'_d - x_{ls}} + \psi_{1d} \frac{x'_d - x''_d}{x'_d - x_{ls}} - V_q \right) \quad (7)$$

$$\frac{dE'_q}{dt} = \frac{1}{T'_{do}} \left[-E'_q + E_{fd} + (x_d - x'_d) \left(I_d + \frac{x'_d - x''_d}{(x'_d - x_{ls})^2} \{ \psi_{1d} - E'_q - I_d (x'_d - x_{ls}) \} \right) \right] \quad (8)$$

$$\frac{dE'_d}{dt} = \frac{1}{T'_{q0}} \left[-E'_d + (x_q - x'_q) \left(-I_q + \frac{x'_q - x''_q}{(x'_q - x_{ls})^2} \{ -\psi_{2q} - E'_d + I_q (x'_q - x_{ls}) \} \right) \right] \quad (9)$$

$$\frac{d\psi_{2q}}{dt} = \frac{1}{T''_{q0}} \left(-\psi_{2q} - E'_d + I_q (x'_q - x_{ls}) \right) \quad (10)$$

$$\frac{d\psi_{1d}}{dt} = \frac{1}{T''_{do}} \left(-\psi_{1d} + E'_q + I_d (x'_d - x_{ls}) \right) \quad (11)$$

$$V_q + jV_d = (V_Q + jV_D) e^{-j\delta} \quad (12)$$

$$I_q + jI_d = (I_Q + jI_D) e^{-j\delta} \quad (13)$$

In this formulation, T_H denotes the electrical torque. The parameters x_d, x'_d, and x''_d represent the synchronous generator reactance along the d-axis, as well as the transient and sub-transient reactance's, respectively. Similarly, x_q, x'_q, and x''_q correspond to the q-axis synchronous, transient, and sub-transient reactance's. The stator current components in the dq reference frame are expressed as I_d and I_q, while ψ''_d and ψ''_q denote the sub-transient electromotive force (EMF) flux linkages along the respective axes. The term x_l defines the armature leakage reactance, and E'_d, E'_q represent the transient EMF components in the dq frame. Furthermore, R_H indicates the armature resistance, and V_d, V_q correspond to the dq components of the terminal voltage. The constants T'_{do} and T''_{do} define the d-axis transient and sub-transient open-circuit time constants, respectively. Equations (2)–(10) describe the dq reference frame of the synchronous generator, whereas the (DQ) frame is associated with the network model. The transformation between these reference frames, as detailed in [25], is essential for interfacing the generator and network. Specifically, the voltage V_{DQ} from the network frame is supplied to the generator, and through the transformations in eqn. (12) and (13), it is converted into the dq frame. Conversely, the generator currents obtained from eqn. (6) and (7) in the dq frame are transformed back into the network (DQ) frame.

3.1. Wind Energy Conversion System (WECS)

The size and variety of wind energy conversion systems (WECS), which include a wind turbine, gearbox, electric generator, and power converter, have increased [26]. Variable-speed operation is possible with the Doubly-Fed Induction Generator (DFIG) system, but frequent maintenance is necessary to minimize mechanical failures [6], [27]. Permanent Magnet Synchronous Generators (PMSG) need controllers and converters for efficient grid integration, utilizing a frequency converter (grid-side or rotor-side converter) before delivering power to the grid [28]. While the rotor-side converter monitors PMSG operation, the grid-side converter uses pulse-width modulation (PWM) converters with voltage sources and DC voltage control to transfer active power [28],[27]. Onshore wind farms are easier to develop [28], but offshore wind farms offer a sustainable solution by harnessing wind over oceans, covering more than 70% of the Earth's surface [29]. Control mechanisms such as grid synchronization, voltage/current controllers, fault ride-through, and Maximum Power Point Tracking (MPPT) ensure stable operation. Wind speeds are classified into three regions: Region 1 (low wind speeds), Region 2 (torque control maximizes power extraction) [40], and Region 3 (pitch controller maintains maximum power) [30]. Wind energy, a crucial [31]. sustainable source, enhances energy security, and reduces reliance on fossil fuels [31]. Wind farms, whether onshore (near coasts or mountains) or offshore (deep-sea), require grid connection for stability and flexibility, with offshore wind capacity increasing globally due to consistent wind availability [32]. Wind turbines convert wind's kinetic energy into mechanical energy, then into electricity via an electric generator, functioning either grid-connected or standalone to power remote areas. Additionally, an increase in kinetic energy corresponds to an increase in wind speed [11], [30], The wind energy conversion systems (WECS) have grown in size and complexity, consisting of a wind turbine, gearbox, electric generator, and power converter [26]. Variable-speed operation is possible with the Doubly-Fed Induction Generator system, but frequent maintenance is

necessary to minimize mechanical failures [27]. Permanent Magnet Synchronous Generators need controllers and converters for efficient grid integration, utilizing a frequency converter (grid-side or rotor-side converter) before delivering power to the grid [28]. All though detailed LVRT control strategies were not the primary focus of this research, the converter-based interface inherently contributes to improved dynamic response and stability of the integrated system. Future studies will investigate advanced LVRT control strategies and their interaction with optimized damping controllers.

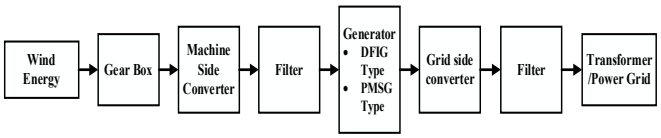

Fig. 5. Wind energy conversion process.

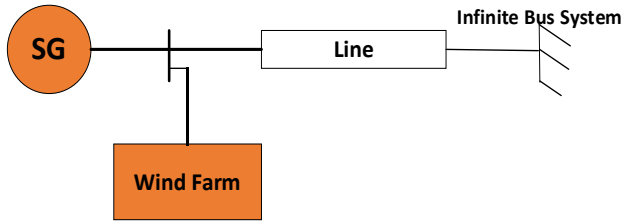

Fig. 6. Integrated system single line diagram.

There are seven parts that make up the DFIG and PMSG with the SMIB network equation: the turbine (aerodynamic and drive train) in eqns. 14-19, the generator in eqns. 20-23, the MSC and B2BC given in eqn. 34, the GSC and MSC obtained in study [24], the filter is given in eqns. 28-33, and network equation 63. The general mathematical equation and data are adopted in study [7], [24].

$$P_T = \frac{1}{2}A_s\rho C_p(\lambda,\beta_p)v_w{}^3 \quad (14)$$

$$C_p(\lambda,\beta_p) = 0.5176\left(\frac{119}{\lambda+0.08\beta} - \frac{4.06}{1+\beta^3} - 0.44\beta\right)e^{\left(\frac{-21}{\lambda+0.08\beta}-\frac{0.735}{1+\beta^3}\right)} + 0.0068\lambda \quad (15)$$

$$\frac{d}{dt}\omega_g = \frac{1}{2H_g}(T_S - T_g) \quad (16)$$

$$T_s = K_{tg}\theta_{tg} + C_{tg}\frac{d}{dt}\theta_g \quad (17)$$

$$\frac{d}{dt}\theta_{tg} = \omega elB(\omega_t - \omega_s) \quad (18)$$

$$\frac{dw_t}{dt} = \frac{1}{2H}(T_m - T_e) \quad (19)$$

$$\frac{L'_s}{\omega elB}\frac{d}{dt}i_{sd} = -\omega_s L'_s i_{sq} - R_1 i_{sd} + \frac{e'_{sq}}{\omega_s T_r} + \frac{\omega_g e'_{sd}}{\omega_s} + v_{sd} + K_{mrr}v_{rd} \quad (20)$$

$$\frac{L'_s}{\omega elB}\frac{d}{dt}i_{sq} = -R_1 i_{sq} + \omega_s L'_s i_{sd} + \frac{\omega_g e'_{sq}}{\omega_s} - \frac{e'_{sd}}{\omega_s T_r} - v_{sq} + K_{mrr}v_{rq} \quad (21)$$

$$\frac{1}{\omega_s \omega elB}\frac{d}{dt}e'_{sd} = -R_2 i_{sq} - \left(1 - \frac{\omega_g}{\omega_s}\right)e'_{sq} - \frac{e'_{sd}}{\omega_s T_r} + K_{mrr}v_{rq} \quad (22)$$

$$\frac{1}{\omega_s \omega elB}\frac{d}{dt}e'_{sq} = R_2 i_{sd} - \frac{e'_{sd}}{\omega_s T_r} + \left(1 - \frac{\omega_g}{\omega_s}\right)e'_{sd} - K_{mrr}v_{rd} \quad (23)$$

$$i_{rq} = -\left(\frac{e'_{sd}}{X_m}\right) - K_{mrr}i_{sq} \quad (24)$$

$$i_{rd} = -\left(\frac{e'_{sq}}{X_m}\right) - K_{mrr}i_{sd} \quad (25)$$

$$\frac{L_i}{\omega_b}\frac{d}{dt}ii_q = v_{iq} - v_{cq} - (R_i+R_c)ii_q + L_i ii_d\omega_g + R_c i_{gq} \quad (26)$$

$$\frac{L_i}{\omega_b}\frac{d}{dt}ii_d = v_{id} - v_{cd} - (R_i+R_c)ii_d + L_i ii_q\omega_g + R_c i_{gd} \quad (27)$$

the inverter side of the filter model

$$\frac{L_g}{\omega_b}\frac{d}{dt}ii_{gq} = v_{cq} - v_{sq} - (R_g+R_c)i_{gq} + L_g i_{gd}\omega_g + R_c ii_q \quad (28)$$

$$\frac{L_g}{\omega_b}\frac{d}{dt}ii_{gd} = v_{cd} - v_{sd} - (R_g+R_c)i_{gd} + L_g i_{gq}\omega_g + R_c ii_q \quad (29)$$

the grid side filter model

$$\frac{C_f}{\omega_b}\frac{d}{dt}v_{cq} = ii_q - i_{gq} + \omega C_f v_{cd} \quad (30)$$

$$\frac{C_f}{\omega_b}\frac{d}{dt}v_{cd} = ii_d - i_{gd} + \omega C_f v_{cq} \quad (31)$$

This B2BC uses the LCL filter to link the rotor windings to the power grid system. Due to the capacitor's dc connection, its voltage can be shown by

$$\frac{1}{C_{dc}}PV_{dc} = \frac{1}{V_{dc}}(P_{msc} - P_{gsc}) \quad (32)$$

Where P_{msc} is the machine side converter active power, P_{gsc} is the grid-side converter active power. The capacitor voltage V_{dc}, the capacitance is C_{dc}.

The PMSG model is similar to the DFIG model, except that it uses a single-mass drivetrain given in eqn. 35, a different generator for PMSG is given eqn. 26-41, These three features distinguish it from the DFIG.

$$\frac{d}{dt}\omega_g = \frac{1}{2H_g}(T_S - T_g) \quad (33)$$

Generator model

The given below where V, φ, ω_{re}, R_a , L, i, $\emptyset_{pm}$ stand for the often use electrical model of PMSG in synchronous reference frame, stator resistance, inductance, current, flux, voltage, flux, and speed in electrical radians/second, respectively.

$$v_d = p\varphi_d - \varphi_q\omega_{re} - R_a I_d \quad (34)$$

$$v_q = p\varphi_q + \varphi_d\omega_{re} - R_a I_q \quad (35)$$

$$\text{where}\varphi_d = -L_d i_d + \emptyset_{pm} \quad \text{and } \varphi_q = -L_q i_q$$

$$L_d pi_d = -v_d + L_q i_q \omega_{re} - R_a i_d \quad (36)$$
$$L_q pi_q = -v_q - L_d i_d \omega_{re} - R_a i_q \quad (37)$$

Network model Let V_b, Z_{net} and i_b be Impedance matrix (13 × 13), current injection vector (13 × 1), and bus voltage vector (13 × 1), correspondingly. Then

$$V_b = Z_{net} i_b \quad (38)$$

$$\begin{bmatrix} V_1 \\ \cdot \\ \cdot \\ V_{12} \\ V_{13} \end{bmatrix} = \begin{bmatrix} Z_{1,1} & \cdot & \cdot & Z_{1,12} & Z_{1,13} \\ \cdot & \cdot & \cdot & \cdot & \cdot \\ \cdot & \cdot & \cdot & \cdot & \cdot \\ Z_{12,1} & \cdot & \cdot & Z_{12,12} & Z_{12,13} \\ Z_{13,1} & \cdot & \cdot & Z_{13,112} & Z_{13,13} \end{bmatrix} \begin{bmatrix} I_1 \\ \cdot \\ \cdot \\ I_{12} \\ I_{13} \end{bmatrix} \quad (39)$$

$$\begin{bmatrix} V_b \\ V_{13} \end{bmatrix} = \begin{bmatrix} Z_A & Z_B \\ Z_C & Z_D \end{bmatrix} \begin{bmatrix} I_b \\ I_{13} \end{bmatrix} \quad (40)$$

Wind turbines generator can be used to determine the current injection at busses 1-6. At busses 7–12, there is no current injection. We are unable to determine the current injection since Bus 13 is an infinite bus (I_{13}) at Bus 13, but we know the voltage (V_{13}). The equation can be rewritten as

$$I_{13} = Z_D^{-1}(V_{13} - Z_C i_b) \quad (41)$$

The network's model representation is shown below.

$$V_b = (Z_A - Z_B Z_D^{-1} Z_C) I_b + Z_B Z_D^{-1} V_{13} \quad (42)$$

The integrated grid single line diagram is shown below in figure 3. bus 13 is the connected to the convectional

3.2. Damping Controller Design

When it comes to the power infusion from renewable energy sources, load changes and power generation upset the equilibrium of a steady electrical power system. A big, networked power system must maintain stability while considering a machine's various rotor angles. By reducing low frequency oscillations, this equilibrium guarantees the stability of the energy system within an acceptable limit of the system's functioning. These oscillations with a low frequency are associated with a collection of electrical power production equipment or synchronous generators. Nonetheless, a machine's electrical torque is made up of two parts: the damping and synchronizing parts. By dampening low voltage, the damping component contributes significantly to the rotor angle stability of a power system study in [14]. To reduce oscillations and enhance and preserve a power system's angle stability, proper system modelling and damping controller mechanisms are necessary. Various techniques have been employed for damping, including PSS. To reduce necessary instability oscillations and enhance power system stability, the PSS lead lag controller works in tandem with the machine's excitation system to regulate the output power by providing an additional synchronizing torque that is in step with speed eccentricity, its multimachine design utilizing local measurements [6].

Many studies use the PSS to improve the damping in the system while using integrated system such as wind turbines. The PSS for the synchronous generator is seen as an additional AVR block that generates a dampening torque component in step with the rotor angle variation. to enhance the system's dynamic performance. PSS is added to the Synchronous Generator and wind energy source. Its goal is to lessen the system's oscillation phases [33], [21]. Linear control theory is used to model power systems around a nominal operating point, but non-linear power systems may not perform optimally across a wide range. PSS structure and parameters are designed to deliver optimal performance [2], [21], [34]. When PSS controller action is included, the damping factor rises, causing the oscillations to stabilize more quickly [33].

The PSS design study in [23][19] represent in the figure bellow. A conventional lead-lag PSS structure is shown above it can be described as

$$V_{si} = K_{pi} \frac{sT_W}{1+sT_W} \left[\frac{1+sT_{1i}}{1+sT_{2i}} \frac{1+sT_{3i}}{1+sT_{4i}}\right] \Delta_{\omega i} \quad (43)$$

The structure consists of a control gain K_{pi}, a washout filter with a time constant T_W, two lead lag blocks for phase compensation with time constants T_{1i}, T_{2i}, T_{3i} and T_{4i} and a limiter. V_{si} is the PSS output signal that goes into the generator exciter input$\Delta_{\omega i}$is the generator speed deviation used as the PSS input signal, The stabilizer gains K_{pi} and the time constants T_{1i}, T_{2i}, T_{3i} and $T_{4i}$are to be determined through optimization Subject to

$0.001 \leq K_{pssi} \leq 50$ and $0.001 \leq T_{1i} \leq 1$, $0.02 \leq T_{2i} \leq 1$, $0.001 \leq T_{3i} \leq 1$ and $0.02 \leq T_{4i} \leq 1$

The optimal value for the PSS obtained using SBO and AEO is in table 2.

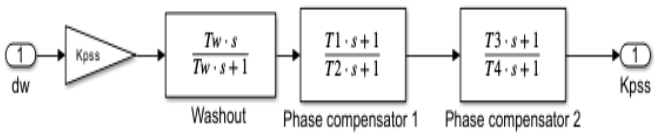

Fig. 7. PSS damping controller connected to the excitation system.

3.3. Objective Function Formulation

The electromechanical oscillation amplitude determines the damping ratio of a system; hence, for the quick attenuation of these oscillations, the PSS damping controller parameters are obtained through optimization. The rotor speed deviation

error results in electromechanical modes of oscillation. Therefore, to control and damp these electromechanical modes of oscillation, the rotor speed deviation error is minimized, which in turn improves the damping ratio. The eigenvalues of the state matrix A and its position on a complex S-plane describe the stability of the linear system, which is in the form of Eqn. 44.

$$\lambda_i = \sigma_i \pm \omega_i \tag{44}$$

where σ_i is the real part that represents damping and ω_i is the imaginary part that gives the oscillation frequency of the eigenvalues. Complex conjugate eigenvalues are used to analyze the behavior of the oscillation, and a negative real part results in decreased oscillation, whereas a positive real part results in increased oscillation. In this study, an eigenvalue objective function was defined to damp the electromechanical modes (EMs) and improve damping in a power grid system by moving the eigenvalues to the region of stability (negative real part of the eigenvalue). This oscillation behavior is expressed on the complex S-plane.

$$J = \max\{\text{real}(\lambda_i)|\lambda_i \in \text{EMs}\} + P_C \sum\{\text{real}(\lambda_j)|\lambda_j > 0\} \tag{45}$$

$$\text{EMs} = \left\{\lambda_k \middle| 0 < \frac{\text{im}(\lambda_k)}{2\pi} < 5\right\} \tag{46}$$

Electromechanical oscillation mode (Ems) are obtained from the imaginary part of conjugate eigenvalues which represent the oscillation frequency [35].Where $\max\{\text{real}(\lambda_i)|\lambda_i \in \text{EMs}\}$ maximizes the damping of the identified electromechanical modes, and $\sum\{\text{real}(\lambda_j)|\lambda_j > 0\}$ prevents the system from having unstable electromechanical modes , P_C is a penalty constant that adjusts the relative importance of the two parts of the objective function, P_C is considered to be 50 [12].

3.4. Secretary Bird Optimization Algorithms

SBOA, a bird-like optimization technique, uses exploration and exploitation phases to search for solutions, resembling hunting behavior. Iterative alternating between phases enhances convergence, accuracy, and stability [6], [36]. The mathematical model equations for the two primary phases of the Secretary Bird Optimization Algorithm (SBOA) are provided below [19].

$$X_{ij} = lb_j + r \times (ub_j - lb_j), i = 1,2,\dots,N, j = 1,2,\dots,Dim \tag{47}$$

ub_j and lb_j are lower and upper bound secretary bird, and r denote the random number from 0-1, The Secretary Bird Optimization Algorithm (SBOA) employs a population-based methodology, whereby optimization begins from a pool of potential solutions, as demonstrated by Equation (1.2). Within the upper and lower bound restrictions for the given issue, these potential solutions X are created at random. Every iteration treats the best answer found so far as about the ideal option.

$$X = \begin{bmatrix} x_{1,1} & x_{1,2} & \cdots & x_{1,j} & \cdots & x_{1,Dim} \\ x_{2,1} & x_{2,2} & \cdots & x_{2,j} & \cdots & x_{2,Dim} \\ \vdots & \vdots & \ddots & \vdots & \ddots & \vdots \\ x_{i,1} & x_{i,2} & \cdots & x_{i,j} & \cdots & x_{i,Dim} \\ \vdots & \vdots & \ddots & \vdots & \ddots & \vdots \\ x_{N,1} & x_{N,2} & \cdots & x_{N,j} & \cdots & x_{N,Dim} \end{bmatrix}_{N\times Dim} \tag{48}$$

N is the secretary bird number. Every secretary bird stands for a potential fix to improve the issue. The values that each secretary bird suggests for the problem variables may thus be used to assess the objective function. Next, a vector is created by compiling the values of the resultant objective function using eqn. 49.

$$F = \begin{bmatrix} F_1 \\ \vdots \\ F_i \\ \vdots \\ F_N \end{bmatrix}_{N\times 1} = \begin{bmatrix} F(X_1) \\ \vdots \\ F(X_i) \\ \vdots \\ F(X_N) \end{bmatrix}_{N\times 1} \tag{49}$$

F is the vector objective function values and F_i represent the objective function collect from i^{th}. The secretary bird's hunting strategy and escape technique are classified into three equal time intervals based on biological statistics, with each stage lasting two distinct times.

$$t < \tfrac{1}{3}T,\ \tfrac{1}{3}T < t < \tfrac{2}{3}T,\ \tfrac{2}{3}T < t < T \tag{50}$$

representing the three phases of the secretary bird's feeding cycle: hunting, consuming, and assaulting prey. As a result, all SBOA processes are modeled. updating the secretary's position when hunting, eating, and attacking prey

$$t < \tfrac{1}{3}T,\ x_{i,j}^{new\ P1} = x_{ij} + (x_{random\_1} - x_{random\_2}) \times R_1 \tag{51}$$

$$\tfrac{1}{3}T < t < \tfrac{2}{3}T,\ x_{i,j}^{new\ P1} = x_{best} + e^{(t/T)^4} \times (RB - 0.5) \times (x_{best} - x_{ij}) \tag{52}$$

$$\tfrac{2}{3}T < t < T,\ x_{i,j}^{new\ P1} = x_{best} + \left(1 - \frac{t}{T}\right)^{\frac{2t}{T}} \times x_{ij} \times RL \tag{53}$$

Where t denoted as the current iteration, T is the max and present iteration number,$x_i^{new\ P1}$ is the update state of i^{th}. x_{random_1} and x_{random_2} are the random candidate in first iteration. All the phases are in the same position X_i of secretary bird i^{th}, R_1 is random generation of array 1 by D from range [0,1], Dim is dimension of solution space, $x_i^{new\ P1}$

is the value of j dimension, and $F_i^{new,P1}$ is the fitness value of objective function

$$X_i = \begin{cases} X_i^{new,P1}, \text{if } F_i^{new,P1} < F_i \\ X_i, \text{else} \end{cases} \quad (54)$$

We apply the weighted Levy combat, often known as RL

$$RL = 0.5 \times Levy(Dim) \quad (55)$$

The Levy combat distribution function is denoted by Levy (Dim). The calculation is as follows
and a fixed constant of 0.01.

$$Levy(D) = s \times \frac{u \times \sigma}{|v|^{\frac{1}{\eta}}} \quad (56)$$

Also η is a 1.5 fixed constant. Two random integers in the interval [0, 1] are u and v. The σ is define as

$$\sigma = \left(\frac{\gamma(1+\eta) \times \sin\left(\frac{\pi\eta}{2}\right)}{\gamma\left(\frac{1+\eta}{2}\right) \times 2\eta\left(\frac{1-\eta}{2}\right)} \right)^{\frac{1}{\eta}} \quad (57)$$

$$\sigma = \left(\frac{\gamma(1+\eta) \times \sin\left(\frac{\pi\eta}{2}\right)}{\gamma\left(\frac{1+\eta}{2}\right) \times 2\eta\left(\frac{1-\eta}{2}\right)} \right)^{\frac{1}{\eta}} \quad (58)$$

Exploration stage: In order to avoid premature convergence to local optima, the algorithm traverses the solution space extensively in the exploration stage, which mimics the hunting activity of secretary birds.

$$\text{Exploration } (\%) = \frac{Div(t)}{Div_{max}} \times 100 \quad (59)$$

Exploitation Stage: The algorithm simulates the bird's flight from predators in this phase, honing and enhancing previously found solutions by concentrating on a more accurate local search to get the best outcomes.

$$\text{Exploitation } (\%) = \frac{|Div(t) - Div_{max}|}{Div_{max}} \times 100 \quad (60)$$

These equations assist SBOA in adaptively alternating between local exploitation and global exploration, guaranteeing a balanced search process of the escape behavior. Dimension diversity Div,t. model

$$Div(t) = \frac{1}{D}\sum_{d=1}^{D} \frac{1}{N}\sum_{i=1}^{N} |median(x_d(t)) - x_d(t)| \quad (61)$$

Secretary birds avoid predators by either flight (C2) or camouflage (C1). This equation dynamically regulates the trade-off between search diversification and solution refining. The following is a mathematical model of these behaviors.

$$X_{i,j}^{new,P1} = \begin{cases} C1: x_{best} + (2 \times RB - 1) \times \left(1 - \frac{t}{T}\right)^2 \times x_{ij} \text{ if } r < r_1 \ (C1) \\ C2: \ x_{ij} + R_2\left(x_{random} - K \times x_{ij}\right), \text{ else } (C2) \end{cases} \quad (62)$$

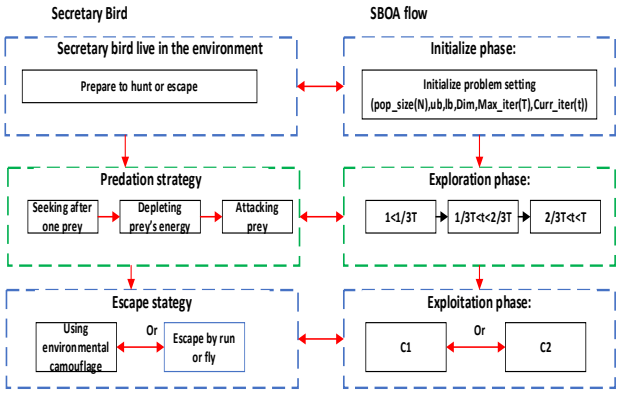

Fig. 8. Secretary bird hunting and escape strategies.

The optimization parameters used in the SBO algorithm were defined with five decision variables (dimension = 5) representing the PSS parameters. The lower bounds were set to [0.01, 0.01, 0.01, 0.01, 0.01], while the upper bounds were [50, 1, 1, 1, 1]. The algorithm was executed with a population size of 50 secretary birds and a maximum of 100 iterations to obtain the optimal solution.

Step-by-step algorithm for designing an optimal power system stabilizer (PSS) using the Secretary Bird Optimization Algorithm (SBOA). The algorithm can update and bound of the variable base on damping controller design.

- Define the PSS design problem by selecting the controller parameters to optimize. Represent each candidate solution as a vector: x = [Kpss, T1, T2, T3, T4] and set the lower and upper bounds for each parameter.
- Randomly initialize a population of candidate solutions within the defined search space.
- Evaluate the fitness of each candidate by simulating the power system (for example, using an SMIB or multi-machine model) and computing the objective function (which may include criteria such as damping ratio improvement, eigenvalue placement, or time-domain error minimization).
- Identify and record the best candidate solution (x_best) from the initial population based on the objective function value.
- **Exploration Phase (Hunting Behavior):**
  a. Update each candidate solution using an exploration operator inspired by the secretary bird's hunting for prey.

- **Exploitation Phase (Evasion Behavior):**
  a. Refine the promising candidate solutions by performing a local search around them.
  b. Update each candidate using a local search operator that mimics the bird's evasion from predators, thereby fine-tuning the solution to move toward a local optimum.
- Re-evaluate the fitness of the updated candidates using the objective function. If any candidate shows improvement over x_best, update x_best accordingly.
- Update the population by replacing inferior candidates with the improved solutions.
- Select the termination criteria (such as maximum number of iterations or a convergence threshold). If the criteria are not met, return to Step 5 and repeat the exploration and exploitation phases.
- Once the termination criteria are satisfied, select x_best as the optimal set of PSS parameters.
- Finally, validate the optimal PSS design through further simulations (e.g., eigenvalue analysis, time-domain response) to ensure it provides the desired damping performance and system stability.

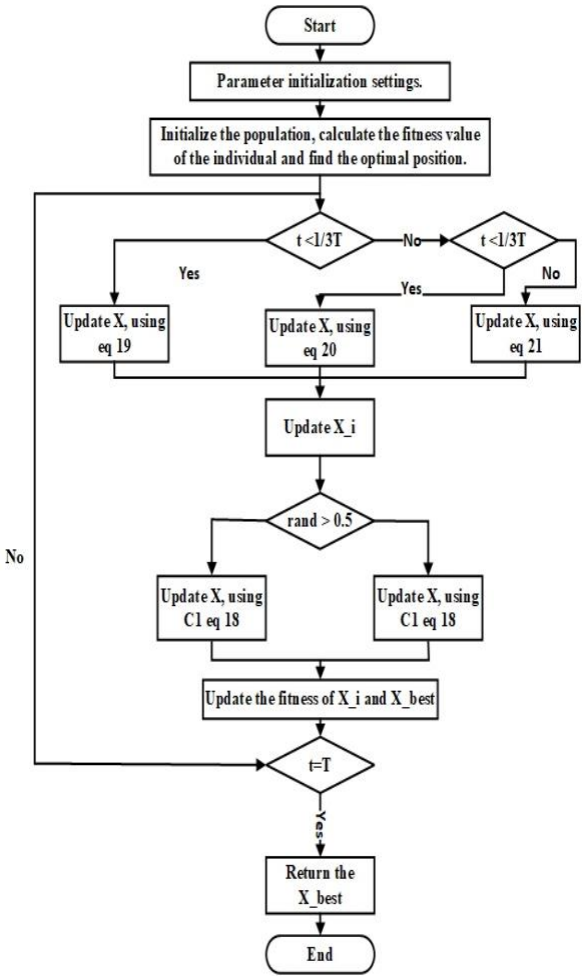

Fig. 9. Flow chart of the secretary bird optimization process for PSS design.

3.5. Artificial Eco-system Algorithm

The basic concept and mathematical expressions of AEO can be seen in the study the steps for AEO application to PSS design are explained below; The steps of the AE algorithm for optimal PSS tuning study in [12],

4. Results

The results obtained from simulations by implementing the various mathematics equations on Matlab/Simulink software. Most importantly, the simulation of the SBO algorithm and its performance evaluation on the test system. The SMIB and WECS system modeled is now used for numerical simulations, The bus data and lines data are adopted from [24]. Introduced a small disturbance of 50% p.u is applied to the mechanical torque input on the generator (conventional system) the generator simulation time is 10 second. The uncontrolled generator rotor speed deviation and rotor angle are displayed in Fig. 11 and Fig. 12 respectively. And Fig. 12 shows Single generator step response uncontrol change in governor load reference

As previously mentioned, the rotor speed deviation in the generator leads to the generator rotor angle deviation, as shown in Fig. 12.

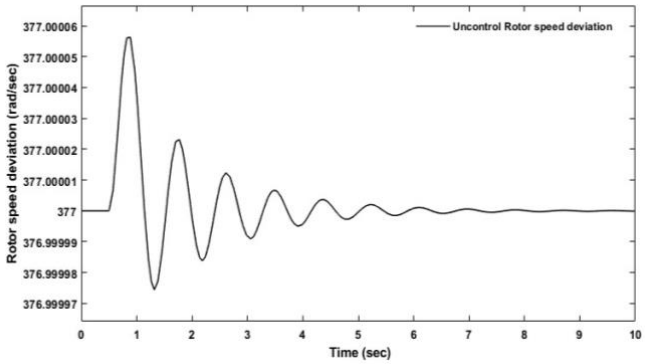

Fig. 10. rotor speed deviation of the synchronous generators.

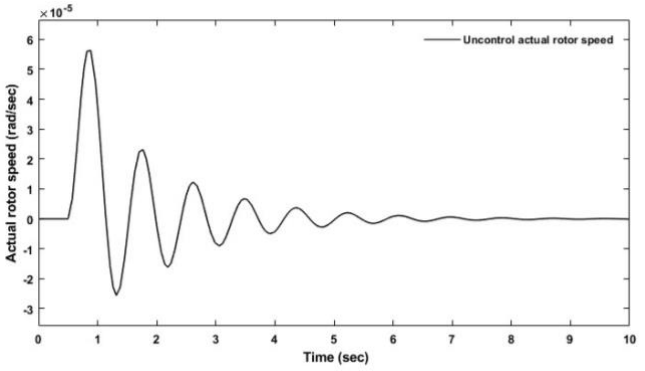

Fig. 11. Actual rotor speed red/sec or p.u.

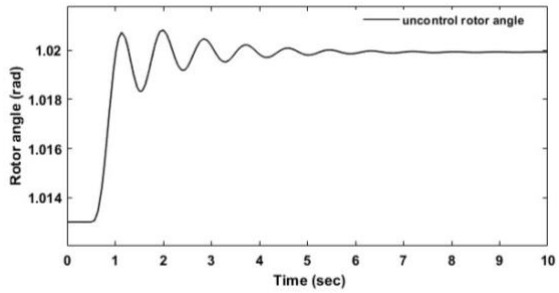

Fig. 12. Generator rotor angle deviation.

When a small step disturbance of 50% p.u. is applied to the mechanical torque input, the mechanical torque temporarily exceeds the electrical torque, creating an accelerating torque that slightly increases the rotor speed. This causes a small rotor speed deviation Δω and a corresponding shift in rotor angle δ.

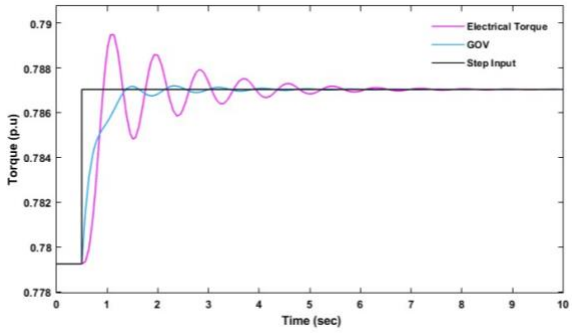

Fig. 13. Single generator step response uncontrol change in governor load reference.

In the No PSS scenario, the system shows a pair of complex eigenvalues (–0.7014 ± j7.2164) with a low damping ratio of 0.0967, signifying inadequate damping and persistent electromechanical oscillations in rotor speed and power output. This result indicates that, in the absence of a damping controller, the system's dynamic stability is weak, making it more susceptible to oscillations when subjected to small disturbances.

Table 1. Eigenvalues of the uncontrolled power system and the corresponding damping ratio

Mode	No PSS	Damping ratio	Frequency
1	-53.8970 + 0.0000i	1.0000	0
2	-34.4672 + 0.0000i	1.0000	0
3	-16.8199 + 9.6223i	0.8680	1.5314
4	-16.8199 - 9.6223i	0.8680	1.5314
5	-0.7014 + 7.2164i	0.0967	1.1485
6	-0.7014 - 7.2164i	0.0967	1.1485
7	-2.9531 + 0.0000i	1.0000	0
8	-4.9866 + 0.0000i	1.0000	0

The convergence rate curve for the PSS design of AEO and SBO is shown in Fig. 12 the curve shows which optimization technique converged faster in optimal PSS design. From the Figure, AEO converged at iteration 32, SBO iteration 20, Thus SBO converged faster. Table 2 below shows the optimal PSS parameters obtained using AEO and SBO algorithms

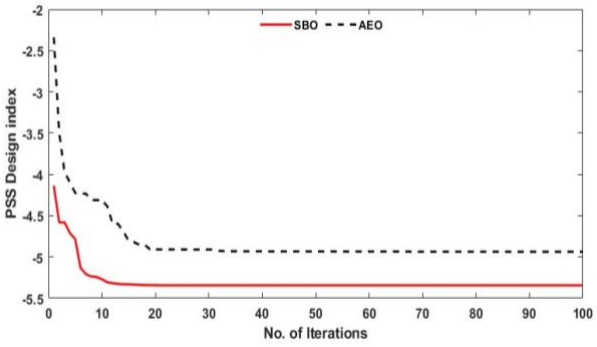

Fig. 14. PSS design convergence rate comparing SBO with AEO.

Table 2. Optimal PSS parameters obtained using AEO and SBO algorithms

Algorithm	AEO	SBO
Kpss	46.254	42.4602
T1	0.0874	0.0697
T2	0.0200	0.0100
T3	0.1036	0.1002
T4	0.0200	0.0100

From Table 3, Δω(t) the generator rotor speed deviation for the No-PSS controller in the system has a settling time of 9.98 seconds out of 10 seconds which is the simulation time. AEO-PSS settles at 3.49 seconds, SBO-PSS at 1.99 seconds, and the generator rotor actual speed has settling time of 2.98 second for AEO, 2.20 second for SBO out of 8.61 second without controller also for the generator rotor angle δ, when there was No-PSS controller in the system, the recorded settling time was 9.41 seconds, with AEO-PSS 3.59 seconds for the SBO-PSS controller 2.21 seconds. And Fig. 19 shows Single generator step response control change in governor load reference with PSS controller. Statistic comparison of settling time for the system is system shows in Fig. 20.

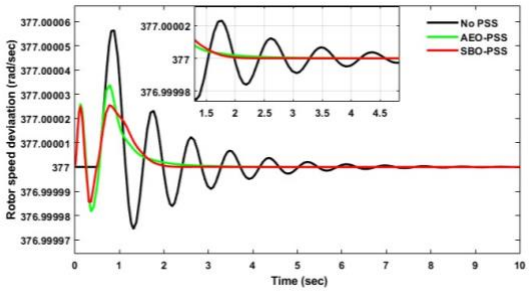

Fig. 15. Control generator rotor speed deviation.

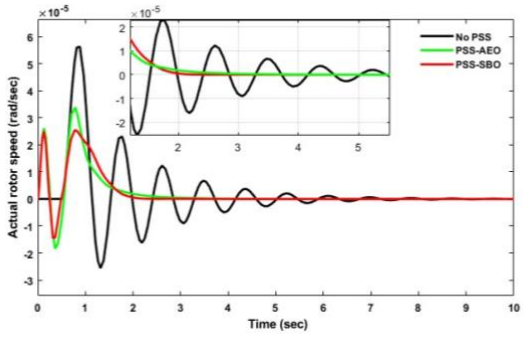

Fig. 16. Control generator actual rotor speed.

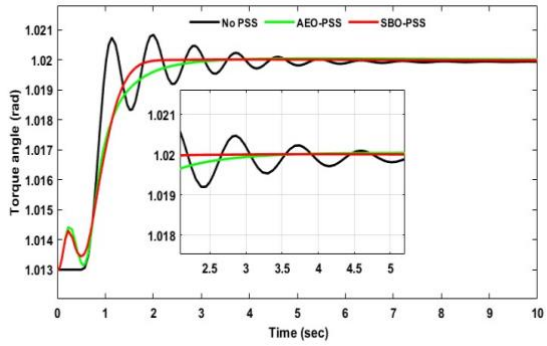

Fig. 17. Controlled generator rotor angle.

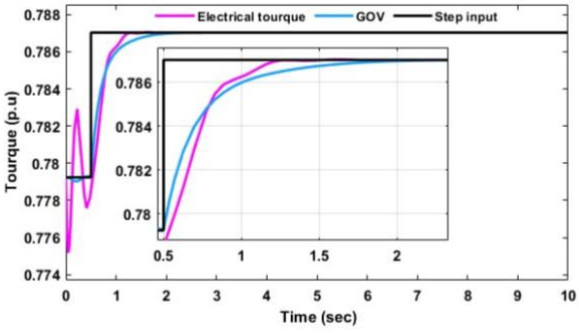

Fig. 18. Single generator step response control change in governor load reference.

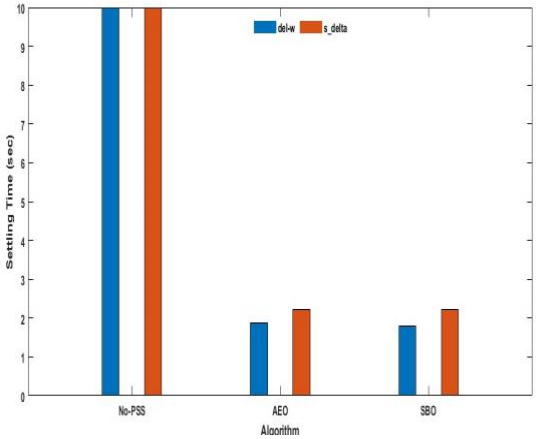

Fig. 19. Statistic comparison of settling time for SMIB system.

A three-phase fault (L-L-L-G) was applied at Bus 2 of the test system for 10 seconds, resulting in a severe grid fault condition. According to the simulation results, when the fault is cleared, the uncontrolled system shows significant oscillations in rotor speed deviation fig.22 and rotor angle fig. 23. Both AEO-PSS and SBO-PSS enhance the system damping performance when the optimized controllers (PSS) are used. the SBO-PSS performs better, lowering oscillation magnitude more successfully and restoring system stability more quickly. Fig. 22 shows the statistic comparison of settling time for SMIB system

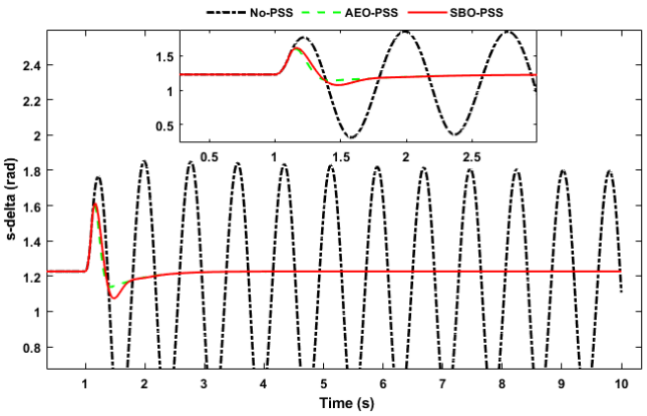

Fig. 20. Control generator rotor speed deviation.

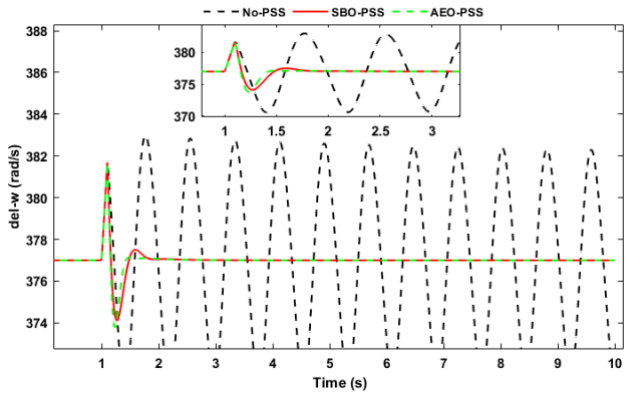

Fig. 21. Controlled generator rotor angle.

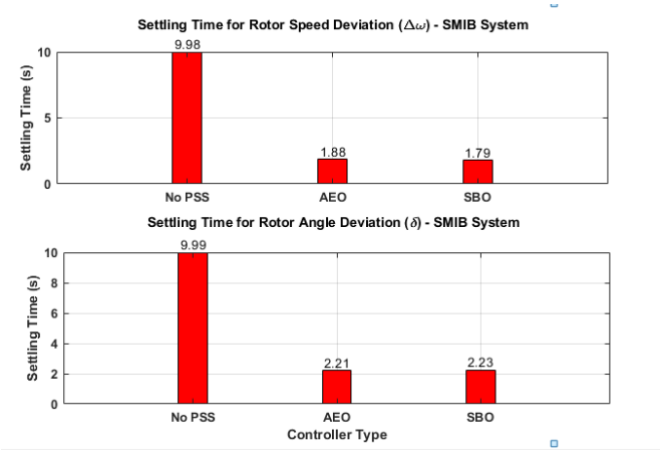

Fig. 22. Statistic comparison of settling time for SMIB system.

Table 3. SMIB test system performance index

	SMIB test System					
	Settling time			Rise time		
Algorithm	No-PSS	AEO	SBO	No-PSS	AEO	SBO
$\Delta\omega(t)$	9.98	3.49	1.99	0.60	0.55	0.50
$\omega(t)$	8.61	2.98	2.20	0.60	0.55	0.50
δ	9.41	3.59	2.21	1.10	0.90	0.85
T_e	7.56					

To quantify the enhancement achieved by the optimized controller configurations, percentage improvement was calculated using the following expression

$$\text{Percentage improvement} = \frac{(\text{Initial value}) - (\text{Improved value})}{(\text{Initial value})} \times 100\% \quad (63)$$

This expression provides a clear measure of how effectively the new controllers (SBO-PSS) enhanced system performance particularly in reducing settling time and improving overall damping compared to the base case without a stabilizer.

Percentage improvement base on AEO-PSS controller

$$\Delta\omega(t) = \frac{(9.98) - (3.49)}{(9.98)} \times 100\% = 65.0\%$$

$$\omega(t) = \frac{(8.61) - (2.98)}{(8.61)} \times 100\% = 65.5\%$$

$$\delta = \frac{(9.41) - (3.59)}{(9.41)} \times 100\% = 61.9\%$$

Percentage improvement base on AEO-PSS controller

$$\Delta\omega(t) = \frac{(9.98) - (1.99)}{(9.98)} \times 100\% = 80.1\%$$

$$\omega(t) = \frac{(8.61) - (2.20)}{(8.61)} \times 100\% = 74.5\%$$

$$\delta = \frac{(9.41) - (2.21)}{(9.41)} \times 100\% = 76.5\%$$

In [37] the settling time after three phase fault occur the rotor speed deviation is 2.6 second, and rotor angle 1.6 second using farmland fertility algorithm. And also in [38] PSO-PSS was used with a settling time of 2.43 second for rotor angle and 1.89 second for rotor speed deviation.

In the new operating condition of the power grid test system eigenvalues with PSS controller modeled on the system. From Table 1, Mode 5 which is for the No-PSS damping controller on the system, following an optimal PSS damping controller design and installation, Mode 5 was improved from -0.7014 +7.2164i to stable mode of -4.7905 -13.1154i for SBO-PSS, -3.5019 -15.6609i for AEO-PSS respectively as shown in Table 4. below. Similarly, the mode 5 damping ratio 0.0967 was improved to 0.34.31 for SBO-PSS, 0.2182for AEO-PSS, respectively. Fig. 21 shows the comparison of eigenvalue plots with AEO-PSS and SBO-PSS damping controller and with a No-PSS damping controller installed on the system. As seen all the eigenvalues for with controller are completely shifts to the left-hand side of the complex S-plane which signifies stability in the system. And Fig. 22 show a damping performance between SBO and AEO.

Table 4. Eigenvalues of the control system and the corresponding damping ratio

Algorithm	AEO-PSS			SBOO-PSS		
Mode	Eigenvalue	Damping ratio	Frequency	Eigenvalue	Damping ratio	Frequency
1	-52.9879 + 0.0000i	1.0000	0	-53.2043 + 0.0000i	1.0000	0
2	-34.7997 + 0.0000i	1.0000	0	-28.4114 + 0.0000i	1.0000	0
3	-29.4720 + 0.0000i	1.0000	0	-34.6931 + 0.0000i	1.0000	0
4	-3.5019 +15.6609i	0.2182	2.4925	-4.7905 +13.1154i	0.3431	2.0874

5	-3.5019 -15.6609i	0.2182	2.4925	-4.7905 -13.1154i	0.3431	2.0874
6	-3.2431 + 2.7533i	0.7623	0.4382	-5.6490 + 5.3320i	0.7272	0.8486
7	-3.2431 - 2.7533i	0.7623	0.4382	-5.6490 - 5.3320i	0.7272	0.8486
8	-0.1016 + 0.0000i	1.0000	0	-1.0923 + 0.0000i	1.0000	0
9	-1.2882 + 0.0000i	1.0000	0	-0.1027 + 0.0000i	1.0000	0
11	-3.3494 + 0.0000i	1.0000	0	-2.7392 + 0.0000i	1.0000	0
12	-4.9887 + 0.0000i	1.0000	0	-4.9864 + 0.0000i	1.0000	0

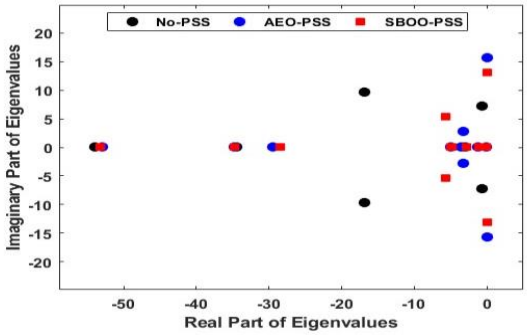

Fig. 23. SBO-controlled PSS system eigenvalues plot compared to NO-PSS controller.

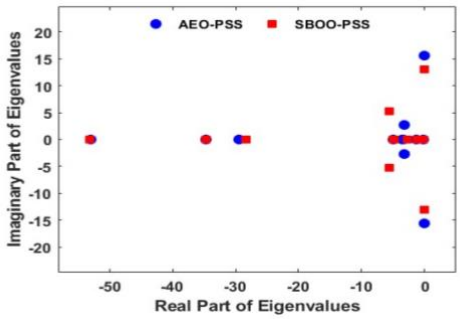

Fig. 24. SBO and AEO PSS system eigenvalue compare damping performance.

The conventional grid and wind energy conversion system parameters respectively. The PSS was tune again to obtain the optimal to enhance the integrated system rotor stability (rotor speed deviation) on the system, Fig. 23 shows the iteration curve of SBO, which converged to its solution at iteration 23.

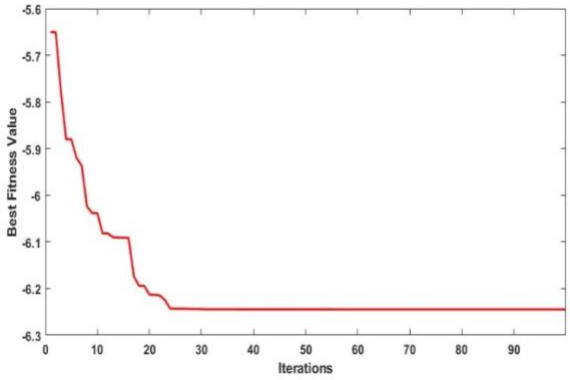

Fig. 25. Iteration curve of SBO.

Table 5. Optimal PSS Parameters Obtained using SBO

Algorithm	Kpss	T1	T2	T3	T4
SBO	32.3581	0.1294	0.4219	0.2401	0.0518

Also, the performance index from the simulation result above for SBO-PSS as regards the settling time and rise time of the generator rotor speed deviation is shown in Table 6.

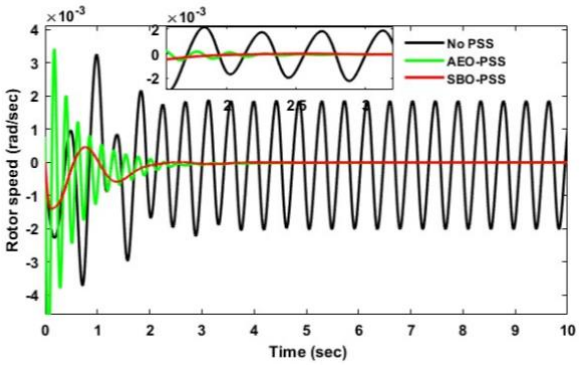

Fig. 26. Integrated system rotor speed response.

From Table 6, ω(t) the generator speed deviation for the SBO-PSS controller in the system has a settling time of 2.20 seconds and 2.51 seconds for AEO-PSS out of 10 seconds which is the simulation time. For the conventional grid with the DFIG and PMSG system, Table 7 shows the dominant eigenvalues for the Electromechanical modes for newly SBO-PSS designed and the corresponding damping ratio. Fig. 25 shows the eigenvalue plot for the integrated system.

Table 6. Integrated system performance index for rotor speed

	Integrated system	
	ω(t) Settling time (sec)	Rising time (sec)
SBO-PSS	2.20	0.31
AEO-PSS	2.51	0.42

Table 7. Integrated system eigenvalue results for the SBO-PSS and the corresponding damping ratio

Mode	SBO-PSS	Damping ratio
01	-14.3743 ±23.1028i	0.0707
02	-27.9085 +0.0000i	1.0000
03	-7.6456 ± 22.6358i	0.3200
04	-48.5978 ± 0.0000i	1.0000
05	-2.0230 + 0.0000i	1.0000
06	-47.8981 + 0.0000i	1.0000

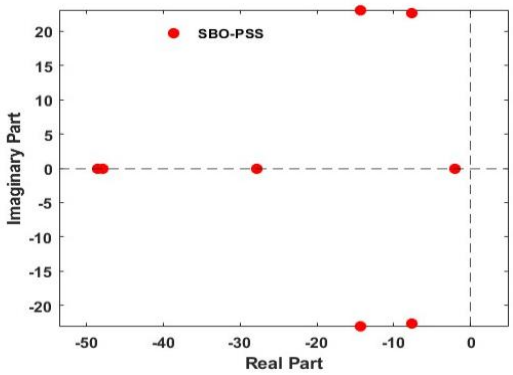

Fig. 27. Eigenvalue plot for SMIB generator with WECS.

5. Conclusion

This paper successfully analyzed and designed an optimized PSS for rotor angle stability enhancement in an integrated power system. By leveraging SBO and AEO optimization algorithms, optimal PSS parameters were obtained to mitigate electromechanical oscillations. The comparative analysis indicates that the SBO-based PSS offers superior performance in terms of faster convergence, better eigenvalue placement, and improved damping characteristics. The results demonstrate that a well-tuned PSS significantly enhances system stability, reducing oscillation magnitude and settling time. The eigenvalue analysis confirms that the optimized PSS effectively shifts dominant poles further into the left half of the complex plane, ensuring improved damping performance. These findings provide a valuable contribution to the field of power system stability, emphasizing the importance of optimization techniques in controller design. Future research will expand the analysis on multi-machine power systems to examine inter-area oscillations and large-scale grid stability, even though the suggested method was verified using a SMIB test system and integrated with wind farms of DFIG and PMSG.

Acknowledgements

The authors gratefully acknowledge the Nigerian Defence Academy (NDA), Kaduna, for offering the academic setting, research facilities, and institutional backing that enabled this study. Appreciation is also extended to the Melbourne Institute of Technology, Australia, and Universiti Putra Malaysia for their technical support, insightful discussions, and collaborative contributions that supported the successful execution of this work. In addition, the authors thank their colleagues and the reviewers for their valuable feedback and recommendations, which significantly enhanced the quality and presentation of this manuscript.

Authors Contributions

D.D carried out the full research work, including problem formulation, system modeling, simulation, data analysis, and manuscript preparation. A.S, K.O, and N.I provided academic supervision, technical guidance, and critical review of the work. A.I contributed as a research colleague through discussions, assistance with simulations, and review of the results.

Conflict of Interest

The authors declare no conflict of interest.

References

[1] B. Desalegn, D. Gebeyehu, and B. Tamirat, "Wind energy conversion technologies and engineering approaches to enhancing wind power generation: A review," *Heliyon*, 2022, doi: 10.1016/j.heliyon.2022.e11263.

[2] A. Sabo, T. E. Odoh, S. Habu, H. Shahinzadeh, and F. Ebrahimi, "A survey of the AVOA metaheuristic algorithm and its suitability for power system optimization and damping controller design," in *Proc. 13th Int. Conf. Computer and Knowledge Engineering (ICCKE)*, 2023, pp. 573–578, doi: 10.1109/ICCKE60553.2023.10326322.

[3] S. D. Ahmed, F. S. M. Al-Ismail, M. Shafiullah, F. A. Al-Sulaiman, and I. M. El-Amin, "Grid integration challenges of wind energy: A review," *IEEE Access*, 2020, doi: 10.1109/ACCESS.2020.2964896.

[4] S. Gawusu, Y. Zhang, F. Ahmed, L. Yu, and X. Xie, "Renewable energy sources from the perspective of blockchain integration: From theory to application," *Sustainable Energy Technologies and Assessments*, vol. 52, 2022, doi: 10.1016/j.seta.2022.102108.

[5] K. E. Okedu and S. M. Muyeen, "Comparative performance of DFIG and PMSG wind turbines during transient state in weak and strong grid conditions considering series dynamic braking resistor," *Energies*, vol. 15, no. 23, 2022, doi: 10.3390/en15239228.

[6] A. Sabo, D. Dahiru, and A. W. Noor Izzri, "A modelling and simulation of damping controller in DFIG and PMSG integrated with a conventional grid: A review," *Vokasi Unesa Bulletin of Engineering, Technology and Applied Science*, vol. 2, no. 2, pp. 148–174, 2025, doi: 10.26740/vubeta.v2i2.34749.

[7] A. Sabo, T. E. Odoh, V. Veerasamy, and N. I. Abdul Wahab, "Modified multimachine power system design with DFIG-WECS and damping controller," *Energies*, vol. 17, no. 8, 2024, doi: 10.3390/en17081841.

[8] W. Aribowo, T. Mzili, and A. Sabo, "Enhanced hippopotamus optimization algorithm for power system stabilizers," *Indonesian Journal of Electrical Engineering and Computer Science*, vol. 38, no. 1, pp. 22–31, 2025, doi: 10.11591/ijeecs.v38.i1.pp22-31.

[9] J. Shair, H. Li, J. Hu, and X. Xie, "Power system stability issues, classifications and research prospects in the context of high-penetration of renewables and power electronics," *Renewable and Sustainable Energy Reviews*, vol. 145, 2021, doi: 10.1016/J.RSER.2021.111111.

[10] S. Impram, S. Varbak Nese, and B. Oral, "Challenges of renewable energy penetration on power system flexibility: A survey," *Energy Strategy Reviews*, vol. 31, 2020, doi: 10.1016/J.ESR.2020.100539.

[11] T. E. Odoh, A. Sabo, N. I. A. Wahab, and A. Wahab, "Mitigation of power system oscillation in a DFIG-wind integrated grid: A review," 2022. [Online]. Available: http://arqiipubl.com/ams

[12] A. Sabo, T. E. Odoh, and N. I. A. Wahab, "Artificial eco-system-based optimization algorithm for optimal design of single-machine infinite bus and multi-machine power system stabilizers," *Electrica*, vol. 23, no. 3, pp. 522–533, 2023, doi: 10.5152/electrica.2023.22228.

[13] A. W. Khawaja, N. A. M. Kamari, and M. A. A. M. Zainuri, "Design of a damping controller using a metaheuristic algorithm for angle stability improvement of an SMIB system," *Applied Sciences*, vol. 12, no. 2, 2022, doi: 10.3390/app12020589.

[14] M. R. Islam, M. T. Hossain, M. A. Rahman, M. S. Islam, and M. A. Rahman, "Power system stability enhancement through optimal PSS design," *e-Prime*, vol. 9, 2024, doi: 10.1016/j.prime.2024.100735.

[15] M. A. El-Dabah, S. Kamel, M. Khamies, H. Shahinzadeh, and G. B. Gharehpetian, "Artificial gorilla troops optimizer for optimum tuning of TID based power system stabilizer," in *Proc. Iranian Joint Congress on Fuzzy and Intelligent Systems (CFIS)*, 2022, doi: 10.1109/CFIS54774.2022.9756463.

[16] A. Sabo, B. Y. Kolapo, T. E. Odoh, M. Dyari, N. I. Abdul Wahab, and V. Veerasamy, "Comprehensive analysis of control strategies and rotor angle stability in hybrid wind energy systems connected to conventional grids," in *Proc. IEEE EPDC*, 2025, doi: 10.1109/epdc67173.2025.11278386.

[17] G. M. Giannuzzi, V. Mostova, C. Pisani, S. Tessitore, and A. Vaccaro, "Enabling technologies for enhancing power system stability in the presence of converter-interfaced generators," *Energies*, 2022, doi: 10.3390/en15218064.

[18] M. A. Hannan, M. A. Hossain Lipu, A. Hussain, M. Saad, A. Ayob, M. M. S. Begum, and T. M. I. Mahlia, "Artificial intelligent based damping controller optimization for the multi-machine power system: A review," *IEEE Access*, vol. 6, pp. 39574–39594, 2018, doi: 10.1109/ACCESS.2018.2855681.

[19] A. A. Alsakati, C. A. Vaithilingam, J. Alnasseir, K. Naidu, and G. Rajendran, "Transient stability enhancement of grid integrated wind energy using particle swarm optimization based multi-band PSS4C," *IEEE Access*, vol. 10, pp. 20860–20874, 2022, doi: 10.1109/ACCESS.2022.3151425.

[20] M. E. C. Bento, "Wide-area measurement-based two-level control design to tolerate permanent communication failures," *Energies*, vol. 16, no. 15, 2023, doi: 10.3390/en16155646.

[21] A. Sabo, B. Y. Kolapo, T. E. Odoh, M. Dyari, N. I. Abdul Wahab, and V. Veerasamy, "Solar, wind and their hybridization integration for multi-machine power system oscillation controllers optimization: A review," *Energies*, 2023, doi: 10.3390/en16010024.

[22] N. Hatziargyriou, J. Milanović, C. Rahmann, V. Ajjarapu, C. Cañizares, I. Erlich, D. Hill, and I. Hiskens, "Definition and classification of power system stability – revisited & extended," *IEEE Transactions on Power Systems*, vol. 36, no. 4, pp. 3271–3281, 2021, doi: 10.1109/TPWRS.2020.3041774.

[23] A. Sabo, T. E. Odoh, and N. I. A. Wahab, "Artificial eco-system-based optimization algorithm for optimal design of single-machine infinite bus and multi-machine power system stabilizers," *Electrica*, vol. 23, no. 3, pp. 522–533, 2023, doi: 10.5152/electrica.2023.22228.

[24] L. Kunjumuhammed, S. Kuenzel, and B. Pal, *Simulation of Power System with Renewables*. Academic Press, 2020.

[25] M. A. Pai, P. W. Sauer, and J. H. Chow, *Power System Dynamics and Stability with Synchrophasor Measurement and Power System Toolbox*, 2nd ed. IEEE Press/Wiley, 2018.

[26] N. Izzri, A. Wahab, T. E. Odoh, and A. Sabo, "Mitigation of power system oscillation in a DFIG-wind integrated grid: A review," 2022. [Online]. Available: http://arqiipubl.com/ams

[27] S. Rajendran, M. Diaz, R. Cárdenas, E. Espina, E. Contreras, and J. Rodriguez, "A review of generators and power converters for multi-MW wind energy conversion systems," *Processes*, 2022, doi: 10.3390/pr10112302.

[28] T. Z. Ang, M. Salem, M. Kamarol, H. S. Das, M. A. Nazari, and N. Prabaharan, "A comprehensive study of renewable energy sources: Classifications, challenges and suggestions," *Energy Strategy Reviews*, vol. 43, 2022, doi: 10.1016/J.ESR.2022.100939.

[29] M. D. Afridi, "Isolated cascaded DAB DC-DC converter to boost medium DC voltage to HVDC," *Quaid-e-Awam University Research Journal*, vol. 21, no. 1, pp. 1–6, 2023, doi: 10.52584/qrj.2101.01.

[30] J. Chen, Y. Fu, D. Liu, and L. He, "Adaptive active fault-tolerant MPPT control of variable-speed wind turbine considering generator actuator failure," *International Journal of Electrical Power & Energy Systems*, vol. 143, 2022, doi: 10.1016/J.IJEPES.2022.108443.

[31] T. Z. Ang, M. Salem, M. Kamarol, H. S. Das, M. A. Nazari, and N. Prabaharan, "A comprehensive study of renewable energy sources: Classifications, challenges and suggestions," *Energy Strategy Reviews*, vol. 43, 2022, doi: 10.1016/J.ESR.2022.100939.

[32] A. Azarpour, O. Mohammadzadeh, N. Rezaei, and S. Zendehboudi, "Current status and future prospects of renewable and sustainable energy in North America: Progress and challenges," *Energy Conversion and Management*, vol. 269, 2022, doi: 10.1016/J.ENCONMAN.2022.115945.

[33] T. E. Odoh, A. Sabo, H. Shahinzadeh, N. I. A. Wahab, and F. Ebrahimi, "DFIG-WECS renewable integration to the grid and stability improvement through optimal damping controller design," in *Proc. ICCKE*, 2023, pp. 547–552, doi: 10.1109/ICCKE60553.2023.10326264.

[34] A. Sabo, N. I. A. Wahab, M. L. Othman, M. Z. A. M. Jaffar, H. Acikgoz, and H. Beiranvand, "Application of neuro-fuzzy controller to replace SMIB and interconnected multi-machine power system stabilizers," *Sustainability*, vol. 12, no. 22, 2020, doi: 10.3390/su12229591.

[35] N. Izzri, A. Wahab, T. E. Odoh, and A. Sabo, "Novel farmland fertility algorithm based PIDPSS design for SMIB angular stability enhancement," *International Journal of Advanced Science and Technology*, vol. 29, no. 6s, pp. 873–882, 2020.

[36] Y. Fu, D. Liu, J. Chen, and L. He, "Secretary bird optimization algorithm: A new metaheuristic for solving global optimization problems," *Artificial Intelligence Review*, vol. 57, no. 5, 2024, doi: 10.1007/s10462-024-10729-y.

[37] A. Sabo, N. I. A. Wahab, M. L. Othman, and M. Z. A. M. Jaffar, "Mitigation of oscillations in SMIB using a novel farmland fertility optimization based PIDPSS," in *Proc. SPIES*, 2020, pp. 234–239, doi: 10.1109/SPIES48661.2020.9242924.

[38] Y. Raghuvamsi, I. Abdul, and C. Rajesh, "Improvement of small signal stability of SMIB system with optimized power system stabilizer," *International Journal of Innovative Technology and Exploring Engineering*, vol. 9, no. 7, pp. 709–716, 2020, doi: 10.35940/ijitee.G5756.059720.